

A concept for calculating accumulated clay thickness from borehole lithological logs and resistivity models for nitrate vulnerability assessment



Anders Vest Christiansen, Nikolaj Foged*, Esben Auken

HydroGeophysics Group, Department of Geoscience, Aarhus University, Denmark

ARTICLE INFO

Article history:

Received 6 September 2013

Accepted 24 June 2014

Available online 30 June 2014

Keywords:

Nitrate vulnerability

Clay thickness

Borehole lithological logs

Resistivity models

ABSTRACT

We present a concept that combines lithological information from boreholes with resistivity information from geophysical data to produce an accumulated clay thickness (ACT) estimate as a proxy for assessing the vulnerability of the groundwater to contamination from nitrate. The groundwater's vulnerability to nitrate is strongly dependent on the hydraulic conductivity and the thickness of the protective layers. Low permeable clays in the overburden offer good protection to underlying aquifers by increasing the transit time. This means that the accumulated clay thickness is a good indicator for aquifer vulnerability to nitrate. In geophysically derived resistivity models clays are characterized by low electrical resistivity, but non-unique clay–sand resistivity transition prevents direct mapping of resistivity models to clay thickness. Within the ACT concept, a translator model linking the resistivity to the accumulated clay thickness is calibrated by borehole information, ensuring consistency between the resistivity and the borehole data. An accumulated clay thickness map of the aquifer overburden (e.g., top 30 m) is then calculated, based on the calibrated translator model and geophysically derived resistivity models. We demonstrate the concept on a large-scale nitrate vulnerability assessment survey in Denmark. The concept successfully delineates the clay-dominated areas that play a key role in the assessment of the aquifer's vulnerability to nitrate pollution.

© 2014 Elsevier B.V. All rights reserved.

1. Introduction

The vulnerability of aquifers in relation to contaminations from land use is a key parameter in areal management (Foster, 1987) in major parts of the world where the supply of drinking water is dependent on groundwater. This is the case in e.g. Europe where approximately 70% of the water supply is based on groundwater (Navarrete et al., 2008) while e.g. in India the percentage is 85%. Contamination often originates from pesticides, fertilizers, or industry. Nitrate is mentioned specifically in the EU Nitrate directive in which member states are required to take appropriate measures to ensure that agricultural nitrate is reduced in the environment and particularly in areas identified as nitrate vulnerable. The vulnerability of an aquifer can be defined as its sensitivity to contamination by surface, or near-surface pollutants (Casas et al., 2008). This definition recognizes that the vulnerability depends on the characteristics of the site; therefore, different soil and hydrogeological settings will result in different amounts of exposure to the aquifer.

A commonly used model to assess groundwater vulnerability to contaminants is the DRASTIC groundwater index (Aller et al., 1987),

which has been customized and applied in a number of different groundwater vulnerability scenarios (Assaf and Saadeh, 2009; Baalousha, 2010; Babiker et al., 2005; Leone et al., 2009). The DRASTIC index includes hydrogeological parameters of (D) depth to water table, (R) recharge, (A) aquifer media, (S) soil media, (T) topography, (I) impact of vadose zone and (C) conductivity (hydraulic). Each category has a rating from 0 to 10 and is assigned different weights resembling its relative importance in the calculation. Boreholes offer many of the key input parameters, but often the spatial density is low and therefore they cannot provide sufficient information to calculate large-scale vulnerability maps with the necessary detail and quality. A higher density can be obtained from geophysical measurements of the resistivity of the subsurface. Especially airborne EM methods are suitable as they map large areas in a short time and by choosing the right system they also have sufficient resolution in the near surface (upper 30 m) needed for the delineation of the geological layers. Dabas et al. (2012) showed how to integrate geophysical results in an indirect way to reach an improved DRASTIC-based vulnerability map. In this case the geophysical results were used to produce a soil map and to confirm and update the geological map of the area. This led to better and more detailed information about the R, S, A, and C parameters in the index.

Kirsch et al. (2003) also use geophysical data, but in a purely geophysically based vulnerability index. Their index is based on a

* Corresponding author. Tel.: + 45 87162378.

E-mail address: nikolaj.foged@geo.au.dk (N. Foged).

summation with depth of the electrical conductance (product of electrical conductivity and layer thickness) of the resistivity models. In this case the resistivity information originated from a helicopter EM survey. Casas et al. (2008) used resistivity information from ground based DC cross sections in an electrical conductance vulnerability index.

Generally, the conductivity (or resistivity) to lithology relationship is quite complex because the formation conductivity is affected by, among other things, porosity, saturation, pore water conductivity, clay content, and clay mineral type with varying Cation Exchange Capacity (CEC). Fundamental empirical models for interpreting resistivity measurements in rocks are Archie's law (Archie, 1942) and the shaly-sands model including the CEC by Waxman and Smits (1968). Site-specific resistivity to lithology relations can be established either based on laboratory measurements or by correlation of the survey resistivities to lithological borehole logs (see Beamish, 2013; Bishop et al., 2001; Mele et al., 2014 for examples).

The geochemical properties of the soil e.g. CEC, pH, and redox conditions are the key parameters in general vulnerability assessment. Many geochemical processes are strongly dependent on the hydrogeological conditions, since the sorption and degradation processes take place during transport from the surface to the aquifers. For nitrate in particular, the parameters that affect the vulnerability are mainly the hydraulic conductivity and the thickness of the overlying geological layers, which define the transport time. For unconsolidated sediments, the hydraulic conductivity is strongly related to the clay content (Kalinski et al., 1993), which to some degree can be deduced from geophysical methods that map the resistivity of the subsurface e.g. direct current (DC) resistivity and electromagnetic (EM) techniques. Though, in near-surface clay layers part of the transport also takes place in macropores of higher hydraulic conductivity extending from the root zone and sometimes down to 10 m depth or more (Jorgensen and Fredericia, 1992).

In Denmark, borehole and resistivity models from DC and time-domain electromagnetic (TEM) data are the primary sources of information for the geological and hydrological models, and thereby also for aquifer vulnerability estimation. Here, we use the accumulated clay thickness in the upper part of the subsurface as an indicator of nitrate vulnerability. The clay content of a formation is strongly correlated with its resistivity, but borehole information is needed to establish the local link between resistivity and lithology, since the resistivity–lithology translation is dependent on the geological environment, and therefore varies laterally. The accumulated clay thickness (ACT) concept presented here combines the two major sources of information, geophysically-derived resistivity models and lithological borehole logs, in an optimization approach (in geophysics termed inversion, in hydrology termed calibration). The resistivity input for the ACT-concept needs to be spatially dense and needs to have a good near-surface resolution. For example this could be resistivity models from airborne frequency domain systems or airborne time domain systems with a high near surface resolution such as the SkyTEM101 system (Schamper et al., 2014). In the field case we used resistivity models from the ground based Pulled Array Continuous Electrical Sounding system (PACES) (Sørensen, 1996) contributing detailed information about the top 20–25 m.

The resulting spatially distributed accumulated clay thickness maps are tailored for vulnerability assessment by combining the locally detailed borehole information with information on the spatial heterogeneity from the geophysics.

2. Methodology

The ACT concept estimates the accumulated clay thickness in a depth interval based on geophysical resistivity models and lithological information from boreholes. It is based on an inversion algorithm, which seeks to minimize the difference between clay thickness observed in boreholes and clay thickness translated from geophysics.

The inversion procedure iteratively updates the model parameters in a geophysical model (the translator model), which converts the geophysical resistivities to meters of clay, seeking the smallest difference between boreholes and geophysics.

The inversion algorithm in its basic form consists of a nonlinear forward mapping of the model to the data space:

$$\delta T_{obs} = \mathbf{G} \delta \mathbf{m}_{true} + \mathbf{e}_{bor} \quad (1)$$

where δT_{obs} denotes the difference between the observed ACT (T_{bor}) and the non-linear mapping of the model to the data space (T_{for}). $\delta \mathbf{m}_{true}$ represents the difference between the true translator model and an arbitrary reference model. \mathbf{e}_{bor} is the observational error, and \mathbf{G} denotes the Jacobian matrix that contains the partial derivatives of the mapping. The general solution to the non-linear inversion problem of Eq. (1) is described in Appendix A, which is based on Auken and Christiansen (2004) and Auken et al. (2005). In the following we will introduce the ACT-concept starting with an over-view followed by a detailed description of each component.

The flowchart in Fig. 1 gives an overview of the ACT-concept, with a detailed description following this overview. Starting from the top in the flowchart: The resistivity models, typically from TEM and/or DC measurements, and the translator model form the forward response, T_{for} (boxes 1, 2 and 3, Fig. 1). The observed clay thicknesses (T_{bor}) and uncertainties (\mathbf{e}_{bor}) are extracted from the lithological log of the boreholes (boxes 4 and 5, Fig. 1). The parameters of the translator model are updated during the inversion to obtain consistency between the T_{for} and the T_{bor} values. The output is an optimum resistivity-to-clay thickness translator model (box 6, Fig. 1). When applying this translator model to the resistivity models, we then obtain the clay thickness map for the survey area (box 7, Fig. 1).

2.1. The translator model

In a sedimentary depositional environment it can be assumed in general that low resistivities correspond to clay or clay rich sediments and high resistivities correspond to non-clay sediments, silt, sand,

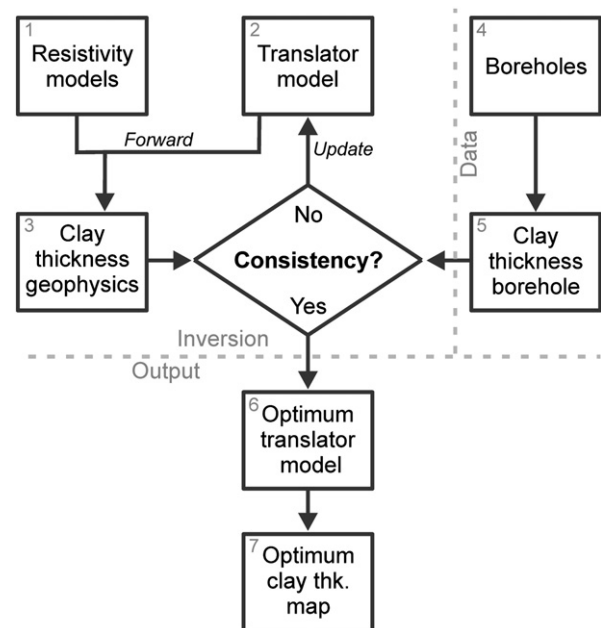


Fig. 1. Flow chart of ACT concept. The translator model (2) is updated until the geophysically-derived clay thickness is consistent with the borehole clay thickness. This optimum translator model (6) is then applied to the resistivity models to achieve the final optimum clay thickness map (7).

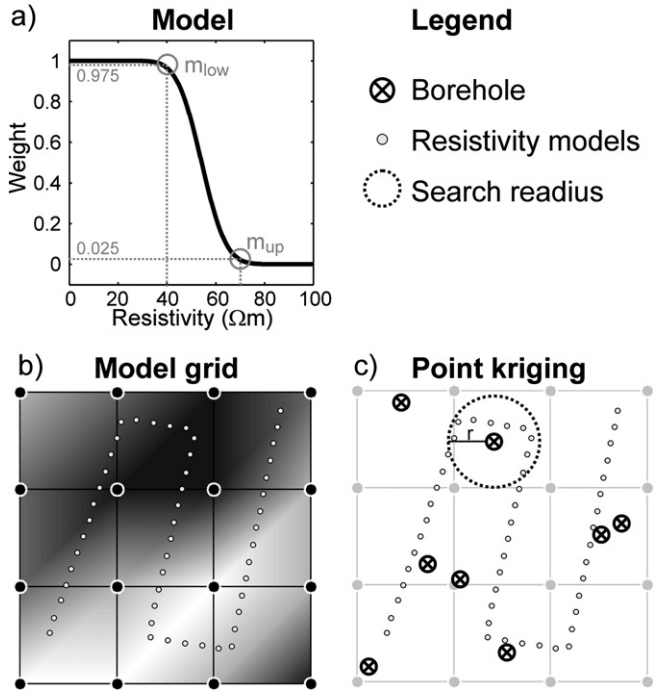


Fig. 2. The translator model and interpolation by point kriging. a) shows the translator model defined by the two resistivity threshold values (m_{low} and m_{up}). b) shows the translator model applied to node points in a grid covering the survey area, enabling unique definition of the translator model anywhere through simple interpolation. c) illustrates the use of point kriging to interpolate the geophysical clay thickness values to the borehole locations.

gravel, chalk etc. Fig. 2a shows the translator model returning a weight, W , between 0 and 1 for a given resistivity value, ρ . The translator model is based on a scaled complementary error function (erfc) defined by a lower resistivity value, m_{low} , and an upper resistivity value; m_{up} . m_{low} and m_{up} represent the clay and sand cutoff values respectively so for resistivity values below m_{low} the layer is counted as clay ($W \approx 1$) and for resistivity values above m_{up} the layer is counted as sand ($W \approx 0$). The translator model ($W(\rho)$) is mathematically defined as:

$$W(\rho) = 0.5 \cdot \operatorname{erfc} \left(\frac{K \cdot (2\rho - m_{up} - m_{low})}{(m_{up} - m_{low})} \right), \quad (2)$$

$$K = \operatorname{erfc}^{-1}(0.0025 \cdot 2)$$

where K scales the complementary error function so that weights of 0.975 and 0.025 are returned for ρ equal to m_{up} and m_{low} , respectively. Using the translator model in Fig. 2a, a 10 m thick layer with a resistivity of e.g. 45 Ω m gets a weight of 0.5 corresponding to clay thickness of 5 m clay for this layer. For a layered resistivity model the clay thickness is then calculated for the N layers and summarized to get the accumulated clay thickness (T_{for}):

$$T_{for} = \sum_i^N W(\rho_i) \cdot t_i, \quad (3)$$

where $W(\rho_i)$ is the clay weight for the resistivity in layer i and t_i is the thickness of the resistivity layer included in the depth interval for the T_{for} calculation. Of course the geophysical resistivity model needs to have a reasonable resolution of the subsurface resistivities in the T_{for} depth interval.

To allow spatial variations in the translator model, a regular model grid is defined for the survey area, each node holding the two parameters of the translator mode (Fig. 2b). A simple bilinear interpolation is used to calculate the parameters of the translator model at the positions of the resistivity models shown with the white dots in Fig. 2b.

2.2. The forward response

As described in the previous section, the first step in calculating T_{for} , is to apply the translator model to the resistivity models. The second step is to interpolate the T_{for} values from the resistivity model positions to the borehole positions (T_{for}^*) for evaluation. The interpolation is performed by point kriging (Fig. 2c), which involves setting a search radius from the estimation points (the borehole positions), and a semi-variogram function. The experimental semi-variogram is calculated based on all the T_{for} values assuming stationarity. Normally the experimental semi-variogram can be approximated well with an exponential function. The search radius depends on the density of the resistivity models and the boreholes and the model grid setup. Typically, a search radius of up to 500 m balances the need for accurate estimations and a fast calculation time of the kriging algorithm. We use the open source geostatistical modeling code Gstat (Pebesma and Wesseling, 1998) for kriging, variogram calculation, and variogram fitting.

The benefits of using kriging for interpolation are that it takes the spatial variance of the T_{for} into account, and as importantly, it also provides uncertainty estimates of T_{for}^* which include the original uncertainty of T_{for} and the interpolation uncertainty. These uncertainty estimates are needed for a meaningful evaluation of the data misfit at the borehole positions.

The variance of T_{for} , $\operatorname{var}(T_{for})$, from Eq. (3) is

$$\operatorname{var}(T_{for}) = \operatorname{var} \left(\sum_{i=1}^N W(\rho_i) \cdot t_i \right). \quad (4)$$

This involves calculating the variance of a sum, a product and the complementary error-function as a function ρ . For a resistivity model, the resistivity and thickness of a layer are often correlated and they are also correlated to the resistivities and thicknesses of the neighboring layers in the model. To make an exact calculation of the T_{for} variance from Eq. (4), we therefore need to know the full covariance matrix of the geophysical model. In some cases we have variance estimates of resistivities and thickness, but the covariances are rarely given by the geophysical inversion routines.

To estimate the T_{for} variance we therefore make the following assumptions:

- The T_{for} variances for resistivities in layers are independent. Presumably, the resistivity variances layer to layer are negatively correlated (increasing the resistivity of one layer can be counterbalanced by a decrease in the next layer to produce the same response) indicating that this assumption results in a conservative variance estimate.
- For a given resistivity layer we neglect the variance of the thickness. Neglecting the variance of the thickness for a few-layered model is a consequence of the first assumption, since an increase in layer thickness of one layer will subsequently lead to a decrease of the thickness for another layer. For a multilayer resistivity model with fixed layer boundaries there is no variance on the thicknesses.

With the assumptions above we can make the error propagation for independent variables (Ku, 1966) and rewrite Eq. (4) as:

$$\operatorname{var}(T_{for}) = \sum_{i=1}^N \left(t_i \cdot \left. \frac{\partial W(\rho)}{\partial \rho} \right|_{\rho=\rho_i} \right)^2 \operatorname{var}(\rho_i). \quad (5)$$

The derivative of the complementary error function is defined as,

$$\frac{\partial}{\partial z} \operatorname{erfc}(z) = -\frac{2}{\sqrt{\pi}} e^{-z^2} \quad (6)$$

and then the weight function differentiated with respect to ρ becomes:

$$\frac{\partial W(\rho)}{\partial \rho} = \frac{-2 \cdot K}{\sqrt{\pi}(m_{up} - m_{low})} e^{-\left(\frac{K(2\rho_i - m_{up} - m_{low})}{(m_{up} - m_{low})}\right)^2} \quad (7)$$

Combining Eqs. (2), (5) and (7) we can then calculate approximate variances for T_{for} .

$$\text{var}(T_{for}) = \sum_{i=1}^N \left[\frac{-2 \cdot K \cdot t_i}{\sqrt{\pi}(m_{up} - m_{low})} e^{-\left(\frac{K(2\rho_i - m_{up} - m_{low})}{(m_{up} - m_{low})}\right)^2} \right]^2 \cdot \text{var}(\rho_i). \quad (8)$$

To the complete variance description of T_{for}^* we add the variance originating from the kriging interpolation itself (Pebesma and Wesseling, 1998).

For a typical setup of boreholes and geophysical models the variance from the kriging will be the dominating part of the total variance of the T_{for}^* values. Hence, the assumptions made above concerning the independency of variables are not crucial for the final inversion results as we will also get reasonable results even if the variances of the geophysical models are unknown.

2.3. Borehole data and uncertainties

The data part in the ACT concept is the accumulated clay thickness observed in the boreholes in a depth interval (T_{bor}) and an uncertainty estimate of T_{bor} . The depth interval corresponds to the T_{for} interval. The T_{bor} data and uncertainty estimates are relatively subjective inputs by the user based on an evaluation of the lithological description from the borehole and the credibility of the sample description. At a first glance, this should be a simple task, but it has proven to be the most time consuming and least objective part of the concept. The lithologies that contribute to the T_{bor} need to be defined. These lithologies are then used to get the most likely T_{bor} value and the uncertainty for boreholes for the depth interval. The uncertainty involves several subjective assessments when evaluating the confidence in the lithological descriptions and borehole meta-data.

For the Danish glacial geology we often have sand, gravel and clays overlying Tertiary deposits of clay or chalk. The clay tills in glacial sequences and the older Tertiary clays are flagged as “protective”. Subjective assessment based on geological knowledge is needed when descriptions such as ‘sandy clay till’ or ‘sand with some thin clay layers’ are encountered and no general rule for handling these cases can be given. For example, for a 10 m thick unit with the description ‘sandy-clay with some thin sand layers’ one would set the T_{bor} value to ~7 m and reflect the inconclusive description in the uncertainty estimate.

3. The Hadsten field case

3.1. The Hadsten area

The Hadsten area is located in the central part of Jutland, Denmark (Fig. 3). The geological setting of the area is a typical glacial landscape formed during the last ice age. The area is intersected by a number of buried valley structures at different levels (some deeper than 100 m) (Jørgensen et al., 2003a,b). The valleys are cut into the underlying sediments mainly heavy paleogene clay and chalk. The in-fill of the valleys consists mainly of quaternary sand and gravel, which form the aquifers. The Hadsten area is important for the groundwater supply, and consists mainly of farmland, with Hadsten as the largest town in the area (population 8,000). The main concern for the groundwater is nitrate leaching from farmland, but also sulfate, chloride and pesticides have been observed close to, and, in some cases, exceeding the maximum levels allowed for drinking water (Rasmussen et al., 2011). The area holds 23 well fields controlled by 19 waterworks, and action



Fig. 3. The black square marks the location of the Hadsten study area.

plans to ensure that the sustainability of the ground water supply is under preparation. A key parameter in the nitrate vulnerability assessment for the area is the ACT map. In the next sections we present data and results from the ACT concept for the case area located south-west of the town of Hadsten (Fig. 4).

3.2. Data and model setup

In this case the subsurface resistivities are measured using the Pulled Array Continuous Electrical Sounding system (PACES) (Sørensen, 1996). The PACES system records eight different 4-pole configurations continuously while pulling the electrodes on the ground surface. The PACES data were processed and inverted with 1D-models with three

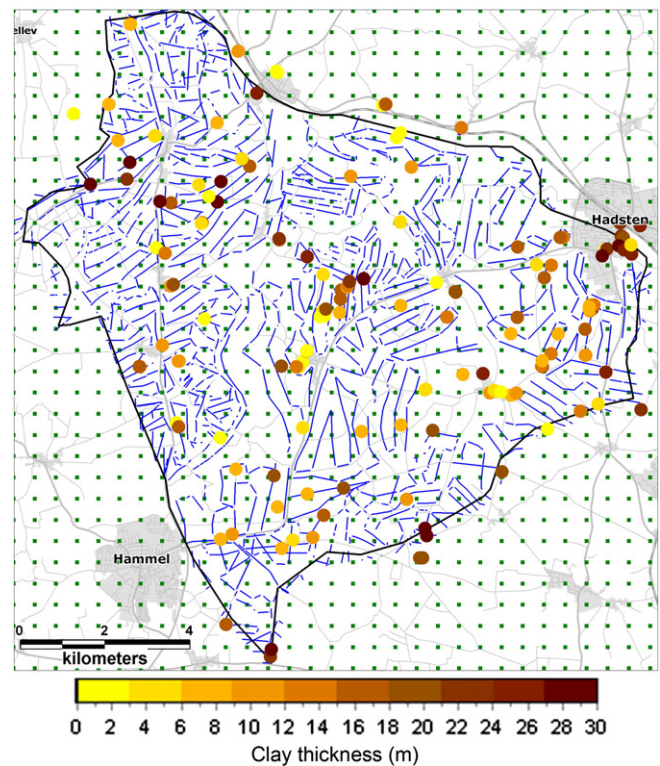


Fig. 4. The Hadsten area. Boreholes are marked with color-coded circles specifying the clay thickness in the upper 30 m. Blue lines mark the positions of the PACES resistivity models. The green dots show the translator model grid.

layers in a laterally constrained inversion setup (Auken et al., 2005). A three-layer model holding five adjustable model parameters (three resistivities and two thicknesses) is the maximum number of degrees of freedom that the PACES data can support in an inversion process. The PACES system provides detailed resistivity information of the upper 20–30 m, and a good spatial resolution is achieved with a line density of approximately 300 m and a model spacing of 10 m along the lines. The PACES lines of the area are shown in blue in Fig. 4, with a coverage of approximately 600 line kilometers, equal to about 60,000 resistivity models.

In Denmark all borehole information is stored in the national database – Jupiter (Møller et al., 2009), dating back to 1926. Today, the database holds information on more than 240,000 boreholes. Each borehole sample in the database is assigned a lithology code from the Danish standard lithology code list. In addition to the lithology code a free-text sample description is available. Using the lithology code, an estimate of the thickness of clay layers can be queried using simple SQL-scripts. Unfortunately, no direct quality parameters or uncertainty numbers exist for the boreholes, the lithology descriptions and the quality of the samples. To identify and exclude the poorest boreholes we have evaluated the meta-data of the boreholes, primarily examining the drilling method and drilling purpose. The color-coded dots in Fig. 4 mark boreholes deeper than 25 m that entered the inversion scheme. The color-coding corresponds to the accumulated clay thickness T_{bor} described in the upper 30 m of the borehole. The input borehole data was prepared in the following way:

- Boreholes with a depth of less than 25 m were excluded.
- Old seismic shotholes and geotechnical boreholes in connection with freeway construction were excluded due to very poor lithological descriptions. The protective clay lithologies were identified and their thicknesses were summarized in the depth interval 0–30 m to obtain T_{bor} .
- The uncertainty of T_{bor} was set ± 2 m, for the boreholes covering the full 30 m depth interval. For boreholes with a drill depth between 25 and 30 m, the uncertainty was increased with the difference between the 30 m and the drill depth.

Some clustering and inconsistent borehole information is observed in Fig. 4, but in general, the spatial distribution of the boreholes is relatively uniform. The maximum interpolation distance of the T_{for} values, for evaluation against the T_{bor} was set to 500 m. Hence, boreholes more than 500 m away from any PACES data do not influence the inversion results and are in reality excluded.

The translator model grid is depicted as green dots in Fig. 4. The full model grid holds 31 times 33 (1023) translator models, with a node spacing of 500 m. The regularization constraint between neighboring nodes is set to a factor of 1.7 meaning that the m_{up} and m_{low} model parameters can vary roughly 70% from one node to the next. A uniform starting model was used with $m_{up} = 50 \Omega$ m and $m_{low} = 70 \Omega$ m respectively. The effective number of translator models within the area covered by PACES measurements is 660 corresponding to 1320 model parameters. The output of the translator models outside the PACES area is purely driven by the model constraints and the starting model, and is therefore not to be considered in the evaluation of the results.

3.3. Results and evaluation

Fig. 5 shows the data residual normalized with the data STD, while the m_{low} and m_{up} parameters defining the optimum resistivity to clay thickness translation are plotted in Fig. 6a and b respectively. The resulting clay thickness map is shown in Fig. 7a. The major part (67%) of the boreholes is fitted within the assumed data error (green dots in Fig. 5), meaning that we obtain a good consistency between the borehole information and the calculated clay thickness from the PACES data. The poorly fitted boreholes, shown with red and purple dots in

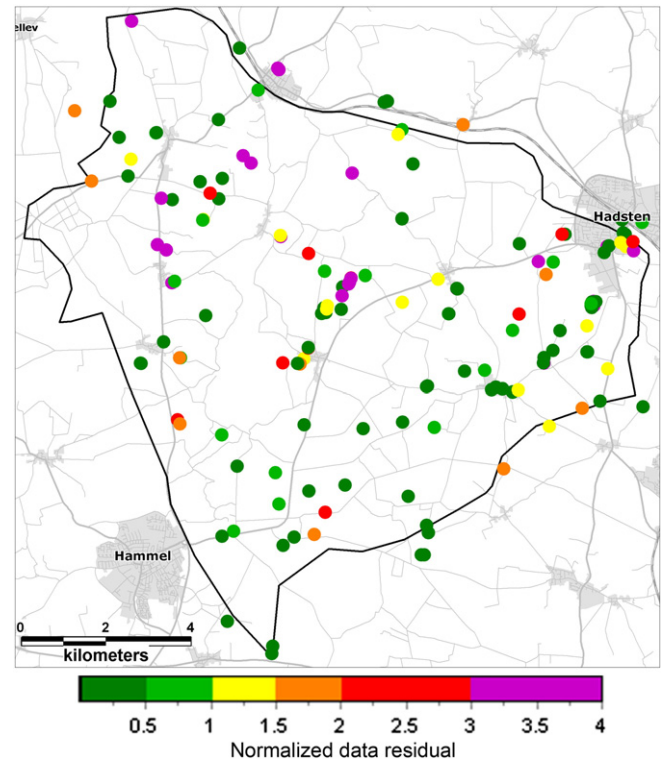


Fig. 5. The colored dots show data residual (data-fit) normalized with the data STD. A data residual of one corresponds to a fit equal to the data STD.

Fig. 5, are mainly placed where the boreholes are clustered and inconsistent borehole information occurs.

Spatial variations of the model parameters are shown in Fig. 6. m_{low} has the lowest values to the north where it ranges from 20 to 30 Ω m and higher values in the range 60–70 Ω m to the east and to the south in the area. The spatial variation of m_{up} is larger than for m_{low} , with values ranging from 30 to 160 Ω m. Especially south-west of Hadsten, we observe high m_{up} parameters, meaning that relatively high resistivities are translated into clay to fit the T_{bor} . This north-south spatial difference in the translator model agrees well with the geological setting. We know that the ice direction was primarily from the north towards the south and that the Paleogene clays are closer to the surface towards the north. The south-moving ice would bring thick clays that would gradually be mixed with other sediments as the ice progressed southwards. This process will produce clays of a lower resistivity to the north than to the south.

The final ACT map in Fig. 7b shows the detailed clay thickness distribution, ranging from areas with no clay in the upper 30 m (yellow color) to areas with thick clay cover (dark brown color). For comparison an ACT map based only on the input borehole data is shown in Fig. 7a. By comparing the ACT maps of Fig. 7a and b, it is clear that the resistivity data provide crucial information to obtain a map with a high level of details. An ACT map based on a fixed translation of only resistivity data (ACT-fixed) has been compiled for comparison and to demonstrate the benefits of the spatially varying translation. The ACT-fixed map was created with a single and fixed threshold value of 60 Ω m. Hence, resistivity values below 60 Ω m are translated into clay for the entire study area. The difference between the ACT-fixed map and the ACT-map of our concept (Fig. 7b) is shown in Fig. 7c. Differences in clay thicknesses in Fig. 7c are observed for large areas with an up to 20 m difference in the clay thickness value, which has a significant impact in a vulnerability estimate. It is worth noting that the 60 Ω m limit chosen for the fixed translation is a qualified threshold value for the Hadsten area, resulting

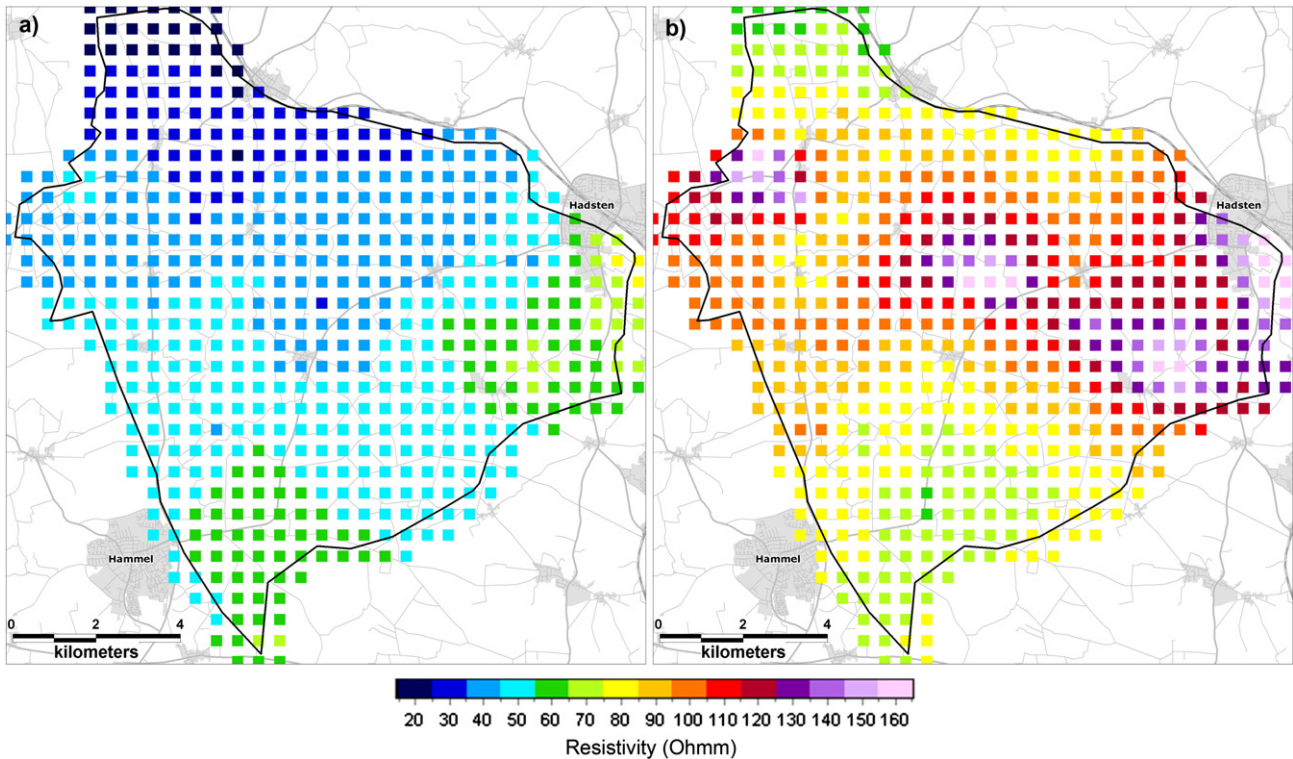


Fig. 6. Inversion results. a) m_{low} parameter of the translator function. b) m_{up} parameter of the translator function. Model nodes outside the survey area are not shown.

in a mean difference close to 0 m when comparing against the ACT map from the approach presented here. The differences would have been larger if other threshold values had been chosen for the fixed translation. Based on Fig. 7 we can conclude that the level of detail in the ACT-map produced by our concept could not have been generated based only on the borehole information, nor could the resistivity data alone have produced a clay thickness map with the same degree of consistency to the borehole observations.

Intensive geophysical and geological mapping has been carried out in large areas both east and west (the study area) of Hadsten town in relation to the mapping of the groundwater resources and their vulnerability. Detailed geological and hydrological models have been set up for the areas, and monitoring data of water quality (nitrate, sulfate, arsenic, carbonate, redox conditions etc.) from the abstraction wells and monitoring wells of the area are also available. In general, the Hadsten area has a high nitrate load. Nitrate leaching from farm land is a great concern and represents a real threat to the primary aquifers. Fig. 8 shows the nitrate concentration (dot size) in different depths (dot color) from water samples in the study area. The European drinking water quality standard for nitrate, which is 50 mg/l, has been exceeded in some of the wells.

Possible land-use regulations to protect and ensure the groundwater resources in the future are based on a nitrate vulnerability map of the area. Fig. 7d shows the two nitrate vulnerability groups namely the *Very vulnerable* (cyan vertical hatching) and the *Vulnerable* (magenta horizontal hatching) areas, as compiled by the Danish groundwater administration. In delineating the vulnerability groups the groundwater administration used the ACT-map in Fig. 7b together with information about:

- Nitrate reduction capacity of the cap layer. A high reduction capacity indicates low vulnerability.
- The nitrate reduction capacity of the water reservoir sediments. A high reduction capacity indicates low vulnerability.
- The quality of the groundwater, especially the oxidized level and concentration of redox ions. A high oxidized level and a high

concentration of redox ions indicate high vulnerability.

- Recharge and the hydraulic gradient. A small or upward going hydraulic gradient indicates low vulnerability.

The ACT-map plays a key role in the delineation of nitrate vulnerable areas as it provides detailed spatial information, while other sources of information such as groundwater quality are only available as point information in some of the boreholes. The role of the ACT-map is clear from Fig. 7d, where the background map is the ACT-map from Fig. 7b. To a large extent the delineation of the of nitrate vulnerable areas follows the areas with low ACT-values.

The comprehensive study and mapping of the groundwater resources and its vulnerability in the Hadsten area have been carried out by the groundwater administration and is reported in Rasmussen et al. (2011).

4. Discussion

When establishing a petrophysical relationship from a limited number of borehole observation points, the question is whether we are representing the true spatial variation in a reasonable way. In a sedimentary setting the resistivity to lithology relationship is controlled primarily by the clay content and the resistivity of the pore water. The spatial variation we observed for the translator model will reflect changes in the pore water resistivity to some extent, but it will also account for the varying resistivity of what is described as “clay in boreholes”, ranging from Paleogene clays with resistivities down to 2 Ω m to firm and dry sandy tills with resistivities up to 80 Ω m.

In the case of salt water affected systems the discrimination between clay and sands may be less clear in the resistivity domain. The ACT-concept can handle changes in the pore water resistivity (salinity) because of the spatially varying resistivity to clay translation. Though, this is only true if the basic assumption of the concept that protective clay layers are more conductive than the permeable sand layers is valid. Furthermore, sufficient borehole information to describe the

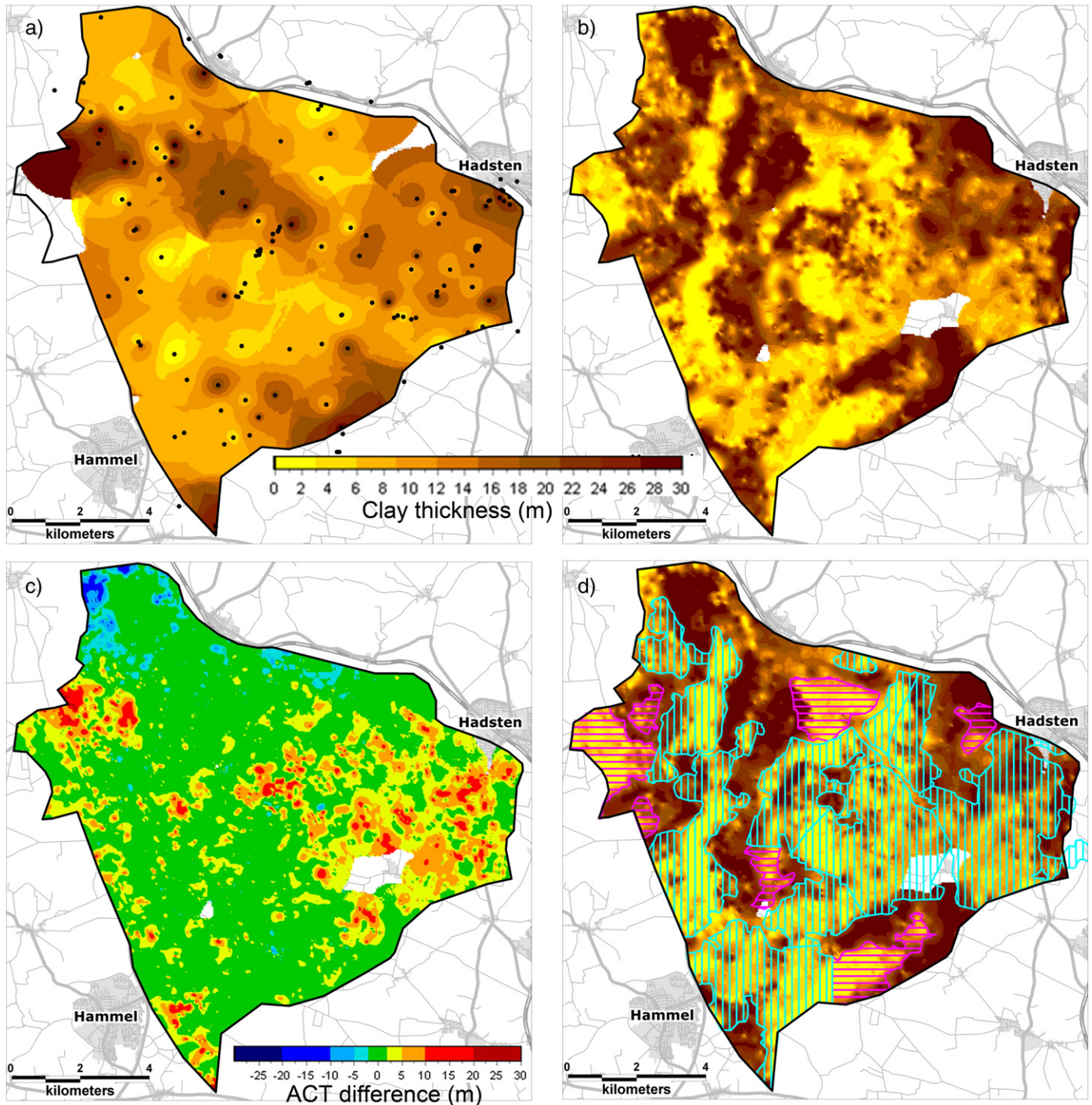


Fig. 7. a) ACT map created by interpolation (inverse distance power 2) of the input borehole data from Fig. 4. b) ACT-map. Kriged grid of the clay thickness values obtained from the resistivity models by applying the spatially varying translator models from Fig. 6. c) Difference in meter clay between the ACT-map in plot b) and an ACT map created by a fixed translation of the resistivity data (not shown). d) Clay thickness map overlain with catchment areas vulnerable to nitrate load. Vertical cyan hatching indicates *very vulnerable* catchment areas and horizontal magenta hatching indicates *vulnerable* catchment areas. Areas without hatching are either not vulnerable or not a catchment area.

effects of the pore water variations on the resistivities of the sand and clay lithologies are required.

The translator models are poorly determined in some cases. Though, in the ACT-concept it is not the translator model itself, but the resulting clay thicknesses that are of interest, and poorly determined translator models do not necessarily result in poorly determined clay thickness estimates. As an example, consider a case where the resistivity distribution is strongly binomial with a clear separation between low resistive clays and high resistive sands. In this case a large variety of translator

models results in the same clay thickness when applied to the resistivity models. Hence the translator models themselves will be very poorly determined, but the estimation of the clay thickness will be well-determined.

The ACT concept has some additional advantages compared to a direct geological interpretation of the resistivity data. Resistivity methods suffer from model equivalences, and this means that in many cases the resistivities and layer thicknesses are poorly determined, but the product or the ratio is well determined. With the ACT concept we are

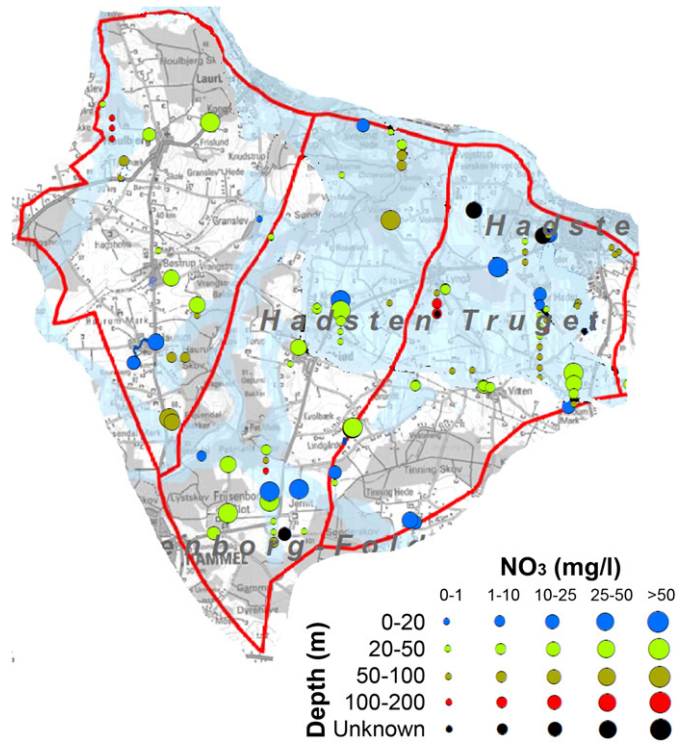


Fig. 8. Nitrate concentration (NO₃) in different depths for the Hadsten area. The dot size indicates the concentration and the dot color specifies the depth of the observation.

working with the product of resistivity and layer thickness (Eq. (3)) and therefore we reduce the model equivalences in the clay thickness output.

The ACT concept is strongly dependent on the quality and density of the boreholes and geophysical data and that an acceptable consistency between the borehole data and the geophysical information is possible. Large misfits might be due to a strongly heterogeneous geology or to saline pore water that violates the basic assumptions. Though in most cases, poorly fitted borehole data are an indication of a low borehole quality.

A more detailed quality ranking of the borehole data could probably provide better uncertainty estimates for the input borehole data. The quality ranking could include parameters like drilling method, drilling purpose, and sample density.

Of course the lateral resolution of our final clay thickness map is strongly dependent on the density and vertical resolution of the geophysical results. For the clay thickness map we can only obtain the same degree of resolution as in the resistivity dataset. In our field case we used PACES resistivity data, but resistivity results from Airborne EM surveys with good near surface resolution e.g. the SkyTEM¹⁰¹ system (Schamper et al., 2014) or a frequency domain system will work as well.

5. Conclusions

We have presented a concept that combines lithological borehole information with geophysical resistivity data to achieve an objective accumulated clay thickness estimate in the subsurface for nitrate vulnerability assessment. The integration of the lithological data and the resistivity models is carried out through inversion, which determines the optimum translator model that describes a simple petrophysical relationship between resistivity and clay thickness. The basic assumption is that low resistivities correspond to protective clays or clayey sediments, and high resistivities correspond to highly permeable non-clay sediments. The inversion concept allows lateral variation in the translation, with smoothness constraints as regularization, and handles

uncertainties on both input and output data. The most time consuming and less objective part of the concept is the description of the clay thickness for the boreholes and the associated uncertainty estimates.

The ACT concept was applied to the Hadsten area for a nitrate vulnerability assessment. Here the clay thickness was estimated in the upper 30 m, which provided a detailed spatial information regarding the aquifers' vulnerability that cannot be obtained with a limited number of boreholes in the area. The final clay thickness map played a key role in the designation of nitrate vulnerable areas. In general the Hadsten area has a high nitrate load, and as a consequence to this, approximately 60% of the area was declared vulnerable to nitrate.

Acknowledgments

The research for this paper has been carried out within the STAIR3D-project (funded by Geo-Center Denmark) and the HyGEM-project (funded by the Danish Council for Strategic Research, DSF 11-116763). We also wish to thank the Danish Ministry of the Environment, The Nature Agency for granting access to data for the field case, and Assoc. Professor Emeritus Niels B. Christensen for inspiring discussion and input, Senior Researcher Verner Søndergaard, now at the Geological Survey of Denmark and Greenland (GEUS), for inspiring us to develop the algorithm in the first place, senior researcher Flemming Jørgensen at GEUS for numerous discussions on borehole descriptions and how to evaluate the results from the ACT algorithm and head of department at GEUS, Flemming Larsen for providing us with valuable insight into nitrate reduction processes in tills and clay formations.

Appendix A

The inversion scheme for the ACT-concept is almost identical to the scheme of the inversion code AarhusInv (Auken et al., accepted for publication) and described in detail in Auken et al. (2005). To solve the inversion problem we minimize the misfit between observed data \mathbf{d}_{obs} having associated errors given by \mathbf{e}_{obs} , and the forward response function $\mathbf{g}(\mathbf{m})$.

In order to solve this problem we use a first order approximation for the non-linear function, g , mapping from model space vectors, m , into data space:

$$\mathbf{d}_{obs} + \mathbf{e}_{obs} \cong \mathbf{G}(\mathbf{m}_{true} - \mathbf{m}_{ref}) + \mathbf{g}(\mathbf{m}_{ref}). \quad (9)$$

Here, \mathbf{m}_{ref} is some reference model vector holding the model parameters of the resistivity to clay translator function, \mathbf{m}_{true} is the true model vector, and \mathbf{G} is the Jacobian matrix. The equation can be further rewritten in terms of successive iterative model updates $\delta\mathbf{m}_{true}$:

$$\mathbf{G}\delta\mathbf{m}_{true} = \delta\mathbf{d}_{obs} + \mathbf{e}_{obs} \quad (10)$$

where $\delta\mathbf{d}_{obs} = \mathbf{d}_{obs} - \mathbf{g}(\mathbf{m}_{ref})$.

The full inversion scheme also includes the regularizing constraints between the model parameters in the model grid and support for a priori information. This is included adding two more sets of equations. The full system of equations can then be stated as:

$$\begin{bmatrix} \mathbf{G} \\ \mathbf{R} \\ \mathbf{I} \end{bmatrix} \delta\mathbf{m}_{true} = \begin{bmatrix} \delta\mathbf{d}_{obs} \\ \delta\mathbf{r} \\ \delta\mathbf{m}_{prior} \end{bmatrix} + \begin{bmatrix} \mathbf{e}_{obs} \\ \mathbf{e}_r \\ \mathbf{e}_{prior} \end{bmatrix} \quad (11)$$

where \mathbf{e}_r is the error on the constraints, with 0 as expected value. $\delta\mathbf{r} = -\mathbf{R}\mathbf{m}_{ref}$ claims identity between the parameters tied by constraints in the roughening matrix \mathbf{R} . \mathbf{I} is the identity matrix, $\delta\mathbf{m}_{prior}$ is a vector identifying the prior model.

These equations are solved in a least squares sense by minimizing the L_2 misfit using an iterative Gauss–Newton minimization scheme with a Marquardt modification. With this approach we obtain a system of linear equations to solve for iterative model updates:

$$\begin{aligned} & (\mathbf{G}^T \mathbf{C}_{obs}^{-1} \mathbf{G} + \mathbf{R}^T \mathbf{C}_c^{-1} \mathbf{R} + \mathbf{C}_{prior}^{-1} + \lambda \mathbf{I}) \cdot \delta\mathbf{m} \\ & = \mathbf{G}^T \mathbf{C}_{obs}^{-1} (\mathbf{d}_{obs} - \mathbf{g}(\mathbf{m}_n)) + \mathbf{R}^T \mathbf{C}_c^{-1} (-\mathbf{R}\mathbf{m}_n) + \mathbf{C}_{prior}^{-1} (\mathbf{m}_{prior} - \mathbf{m}_n). \end{aligned} \quad (12)$$

Here, \mathbf{m}_n is the model vector for the n 'th iterative step, and $\delta\mathbf{m}$ the model update for the next iteration. \mathbf{C}_{obs} , \mathbf{C}_{prior} and \mathbf{C}_c are diagonal covariance matrices holding the uncertainty on the observed data, prior model and constraints, respectively. λ is a Marquardt damping parameter (Marquardt, 1963). During each iteration of the inversion a line search is performed, solving the system for different values of λ until a model update of suitable magnitude is found.

Estimation of the uncertainty for the model parameters can be obtained by the linearized covariance matrix \mathbf{C}_{est} , calculated from the following expression (Tarantola and Valette, 1982):

$$\mathbf{C}_{est} = \left(\mathbf{G}^T \mathbf{C}_{obs}^{-1} \mathbf{G} + \mathbf{R}^T \mathbf{C}_c^{-1} \mathbf{R} + \mathbf{C}_{prior}^{-1} \right)^{-1}. \quad (13)$$

In our case the inversion is performed in logarithmical model space to prevent negative model parameters.

References

Aller, L., Bennett, T., Lehr, J.H., Petty, R.J., Hackett, G., 1987. DRASTIC: a Standardized System for Evaluating Ground Water Pollution Potential Using Hydrogeologic Settings: US EPA, 600/2-87-035.
 Archie, G.E., 1942. The electrical resistivity log as an aid in determining some reservoir characteristics. *Trans. AIME* 146, 54–62.

Assaf, H., Saadeh, M., 2009. Geostatistical assessment of groundwater nitrate contamination with reflection on DRASTIC vulnerability assessment: the case of the upper litani basin, Lebanon. *Water Resour. Manag.* 23, 775–796.
 Auken, E., Christiansen, A.V., 2004. Layered and laterally constrained 2D inversion of resistivity data. *Geophysics* 69, 752–761.
 Auken, E., Christiansen, A.V., Jacobsen, B.H., Foged, N., Sørensen, K.I., 2005. Piecewise 1D laterally constrained inversion of resistivity data. *Geophys. Prospect.* 53, 497–506.
 Auken, E., Christiansen, A.V., Kirkegaard, C., Fiandaca, G., Schamper, C., Behroozmand, A.A., Binley, A., Nielsen, E., Effersø, F., Christensen, N.B., Sørensen, K.I., Foged, N., Vignoli, G., 2014. An overview of a highly versatile forward and stable inverse algorithm for airborne, ground-based and borehole electromagnetic and electric data. *Explor. Geophys.* (accepted for publication).
 Baalousha, H., 2010. Assessment of a groundwater quality monitoring network using vulnerability mapping and geostatistics: a case study from Heretaunga Plains, New Zealand. *Agric. Water Manag.* 97, 240–246.
 Babiker, I.S., Mohamed, M.A.A., Hiyama, T., Kato, K., 2005. A GIS-based DRASTIC model for assessing aquifer vulnerability in Kakamigahara Heights, Gifu Prefecture, central Japan. *Sci. Total Environ.* 345, 127–140.
 Beamish, D., 2013. Petrophysics from the air to improve understanding of rock properties in the UK. *First Break* 31, 63–71.
 Bishop, J., Sattel, J., Munday, T., 2001. Electrical structure of the regolith in the Lawlers District, Western Australia. *Explor. Geophys.* 32, 20–28. <http://dx.doi.org/10.1071/EG01020>.
 Casas, A., Himi, M., Diaz, Y., Pinto, V., Font, X., Tapias, J.C., 2008. Assessing aquifer vulnerability to pollutants by electrical resistivity tomography (ERT) at a nitrate vulnerable zone in NE Spain. *Environ. Geol.* 54, 515–520.
 Dabas, M., Jubeau, T., Rouiller, D., Larcher, J.M., Charriere, S., Constant, T., 2012. Using high-resolution electrical resistivity maps in a watershed vulnerability study. *First Break* 30, 51–56.
 Foster, S.S.D., 1987. Fundamental concepts in aquifer vulnerability, pollution risk and protection strategy. In: van Duijvenbooden, W., van Waegeningh, H.G. (Eds.), TNO Committee on Hydrological Research: the Hague, Vulnerability of Soil and Groundwater to Pollutants. *Proc Inf.* 38, pp. 69–86.
 Jørgensen, P.R., Fredericia, J., 1992. Migration of nutrients, pesticides and heavy metals in fractured clayey till. *Geotechnique* 42, 67–77.
 Jørgensen, F., Lykke-Andersen, H., Sandersen, P., Auken, E., Nørmark, E., 2003a. Geophysical investigations of buried Quaternary valleys in Denmark: an integrated application of transient electromagnetic soundings, reflection seismic surveys and exploratory drillings. *J. Appl. Geophys.* 53, 215–228.
 Jørgensen, F., Sandersen, P., Auken, E., 2003b. Imaging buried Quaternary valleys using the transient electromagnetic method. *J. Appl. Geophys.* 53, 199–213.
 Kalinski, R.J., Kelly, W.E., Pesti, G., Pesti, B., 1993. Electrical resistivity measurements to estimate travel times through unsaturated ground water protective layers. *J. Appl. Geophys.* 30, 161–173.
 Kirsch, R., Sengpiel, K.P., Voss, W., 2003. The use of electrical conductivity mapping in the definition of an aquifer vulnerability index. *Near Surf. Geophys.* 1, 13–19.
 Ku, H.H., 1966. Notes on the use of propagation of error formulas. *J. Res. Natl. Bur. Stand.* 70C.
 Leone, A., Ripa, M.N., Uricchio, V., Deák, J., Vargay, Z., 2009. Vulnerability and risk evaluation of agricultural nitrogen pollution for Hungary's main aquifer using DRASTIC and GLEAMS models. *J. Environ. Manag.* 90, 2969–2978.
 Marquardt, D., 1963. An algorithm for least squares estimation of nonlinear parameters. *SIAM J. Appl. Math.* 11, 431–441.
 Mele, M., Inzoll, S., Giudici, M., Bersezio, R., 2014. Relating electrical conduction of alluvial sediments to textural properties and pore-fluid conductivity. *Geophys. Prospect.* 62, 631–645. <http://dx.doi.org/10.1111/1365-2478.12102>.
 Møller, I., Verner, H., Søndergaard, V.H., Flemming, J., Auken, E., Christiansen, A.V., 2009. Integrated management and utilization of hydrogeophysical data on a national scale. *Near Surf. Geophys.* 7, 647–659.
 Navarrete, C.M., Olmedo, J.G., Valsero, J.J.D., Gómez, J.D.G., Espinar, J.A.L., Gómez, J.A.D.L.O., 2008. Groundwater protection in Mediterranean countries after the European water framework directive. *Environ. Geol.* 54, 537–549.
 Pebesma, E.J., Wesseling, C.G., 1998. Gstat: a program for geostatistical Modelling, prediction and simulation. *Comput. Geosci.* 24, 17–31.
 Rasmussen, S., Nyholm, T., and Nielsen, E., 2011. Afgiftfinansieret grundvandskortlægning - Redegørelse for Hadsten-området Abbott, S., Ed., Danish Ministry of the Environment, ISBN: 978-87-92227-23-2, Danish Ministry of the Environment, ISBN: 978-87-92227-23-2.
 Schamper, C., Auken, E., Sørensen, K.I., 2014. Coil response inversion for very early time modelling of helicopter-borne time-domain electromagnetic data and mapping of near-surface geological layers. *Geophys. Prospect.* <http://dx.doi.org/10.1111/1365-2478.12104>.
 Sørensen, K.I., 1996. Pulled array continuous electrical profiling. *First Break* 14, 85–90.
 Tarantola, A., Valette, B., 1982. Generalized nonlinear inverse problems solved using a least squares criterion. *Rev. Geophys. Space Phys.* 20, 219–232.
 Waxman, M.H., Smits, L.J.M., 1968. Electrical conductivities in oil-bearing shaly sands. *Soc. Pet. Eng. J.* 8, 107–122.